

# USER-FRIENDLY SOFTWARE FOR SIMULATION OF ANODE BAKING FURNACES

Dagoberto S. Severo and Vanderlei Gusberti.  
CAETE Engenharia, Rua Caeté 162, Porto Alegre RS, Brazil  
[caete@caetebr.com](mailto:caete@caetebr.com)

## Abstract

In modern smelters the anode represents from 15 to 25% of the total aluminium production cost [1]. So an optimum operation of the anode baking furnace is important to keep this cost as low as possible.

A thermal transient numerical model of an open-top baking furnace was developed. The balance equations for heat transfer, species concentrations and pressure distribution are solved numerically using the finite volume method. The model takes into account the anode geometry, fluewall hydraulic resistance, air infiltration, combustion of volatile matter, and heat losses. Real furnace measurements are presented and compared with software results showing good agreement.

A user-friendly software for predicting the anode baking process was developed. The user can modify operating parameters such as fire cycle, baking curve, gas massflow, obtaining the new resulting situation in terms of final anode baking temperature. Also the impact of different anode sizes can be studied. The software is a useful tool for the optimization of the anode baking process.

Keywords: anode baking furnace, heat balance, numerical simulation.

## Introduction

The anode baking is the most expensive step in anode production. Fuel and refractory maintenance represent approximately 15% of total anode manufacturing cost [1]. The baking of the anode is completed in an anode ring furnace. Such furnaces are composed of a number of sections with the anodes placed between fluewalls into the pit. The firing zone is moving and the anodes remain stationary. Usually, each furnace has two to four fire groups. Each fire group is composed of typically 10 to 16 sections: three to four anode preheating sections, three to four firing sections and four to nine anode cooling sections. Figure 1 shows the section and peephole scheme used in this paper.

The process starts by placing green anodes into the pit at the ambient temperature. The anodes will reach around 600°C at the end of the preheating. They continue heating up to around 1100°C in the fire sections. Then the baked anodes cool down in the cooling sections, heating the gas before it enters into the fire sections. The entire process takes about 240 to 360 h.

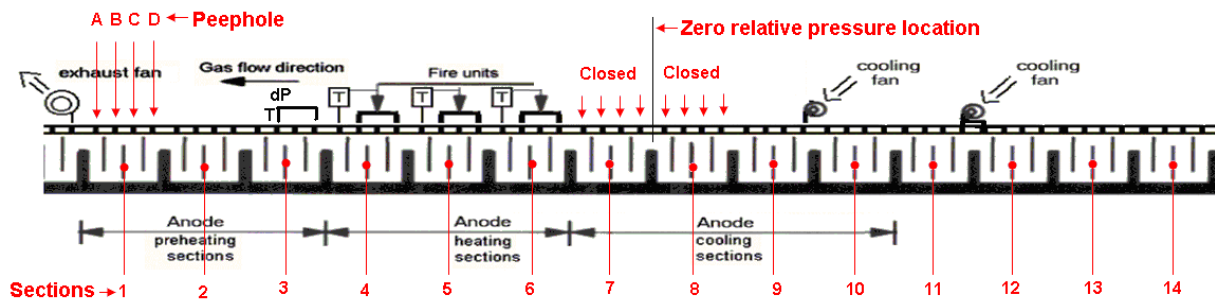


Figure 1 - Anode Baking Furnace Sections and Peepholes Scheme.

Many mathematical models of baking furnaces have been published. Some of these focus on the furnace operation, for example the models presented R.T. Bui et al [2] and R. Ouellet et al [3]. These models are one or two dimensional and simulate the dynamics of the process. Other more detailed models are three dimensional and are used for furnace design or specific studies of part of the process [4, 5 and 8].

In this paper we present a bi-dimensional transient model of an entire fire group for a horizontal open-top ring furnace and show how this model could help to improve the baking process. Balance equations for heat transfer, species concentrations and pressure distribution are solved by dedicated software, built on a Fortran platform. Heat losses, insulation, combustion and fluid flow characteristics of the flue wall are included in the model by running a more complex 3D model as presented in [8].

This model was used and validated in ten different furnaces. Some results of simulations using this software are presented here and have been presented previously in two other papers [9, 10].

## Mathematical Model

The anode baking furnace can be understood as a counter-flow heat and mass exchanger. The gases flow from the cooling sections towards the preheating sections with a velocity determined by local pressure, temperature and infiltration conditions. The movement of the solids occurs in discrete steps equal to the section cycle time in the opposite direction to the gas flow. The real transient effect of the fire and manifold movement is taken into account as the model is a true transient model inside each fire cycle and the fire movement occurs in a discrete way. The Finite Volume Method is used for the evaluation of the balance equations.

In the real furnace, at the end of each cycle period, the manifold and fire bridges are moved. In the model, this is done virtually using a coordinate transformation technique. The model is transient and calculates many cycle times in sequence until convergence is achieved. The model is declared converged when all temperatures of gas and anode pack repeat themselves after exactly one cycle period. Consequently, all the results are valid for “stable” furnace operation.

### Geometric Simplifications

The global model uses a bi-dimensional mesh representing a horizontal slice of the sections directly involved in the process (preheating, firing, cooling). Symmetry is adopted in the pit center plane and flue center plane. Heat conduction inside the solids is calculated in 2D, but heat balance, oxygen concentration (and also CO<sub>2</sub>, H<sub>2</sub>O) inside the flue are evaluated in one-

dimensional form because the variations could be considered small in the flue width direction. Figure 2 presents a schematic view of the model's domain.

The heat losses to the environment occur at the furnace top, and part of the heat is also lost to the bottom. These losses are taken into account in the modeling by imposing appropriate heat loss coefficients. These coefficients are calculated using conductive-convective 3D sub-models that must be validated for every furnace.

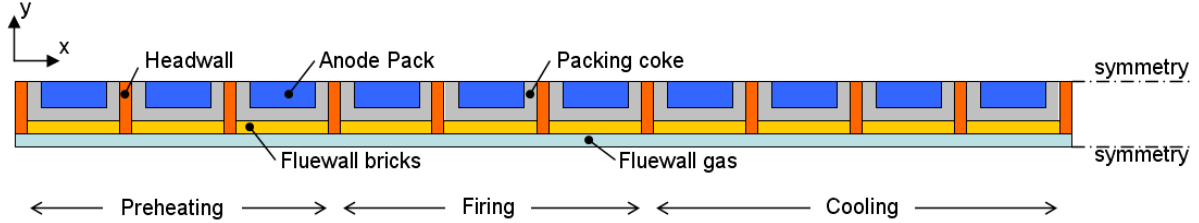


Figure 2 - Schematic View of the Model's Domain.

### Governing Equations

The model is based upon energy and mass balance equations. For the solid parts of the model a 2-dimensional diffusion equation is solved by the classical Finite Volume Method.

$$k \left( \frac{\partial^2 T}{\partial x^2} + \frac{\partial^2 T}{\partial y^2} \right) - Q_s = \rho c \frac{\partial T}{\partial t} \quad (1)$$

Where:

- $k$  is the thermal conductivity of the solids (bricks, coke, anodes) [ $\text{W}\cdot\text{m}^{-1}\cdot\text{°C}^{-1}$ ];
- $\rho$  is the solids density [ $\text{kg}/\text{m}^3$ ];
- $c$  is the solids specific heat [ $\text{J}\cdot\text{kg}^{-1}\cdot\text{°C}^{-1}$ ];
- $x$  is the longitudinal coordinate parallel to the fire direction [m];
- $y$  is the transversal coordinate perpendicular to fire direction [m];
- $t$  stands for time [s];
- $Q_s$  represents the thermal loss to the atmosphere by coke and the foundation [ $\text{W}/\text{m}^3$ ];
- $T$  is the solids temperature [ $\text{°C}$ ].

The boundary conditions applied are:

- At symmetries, heat flux equals zero:

$$\frac{\partial T}{\partial n} = 0 \quad (2)$$

Where:

- $n$  in the normal vector pointing to the boundary outside.

- At the boundaries, where solids and flue gases are in contact, heat is exchanged following the relationship:

$$q'' = (h_C + h_R)(T_g - T_w) \quad (3)$$

Where:

- $q''$  is the heat flux through the fluid-solid interface [ $\text{W}/\text{m}^2$ ];
- $h_C$  is the convection heat transfer coefficient between wall and gas [ $\text{W}\cdot\text{m}^{-2}\cdot\text{°C}^{-1}$ ];

- $h_R$  is the radiation heat transfer coefficient between wall and gas [ $\text{W}\cdot\text{m}^{-2}\cdot^\circ\text{C}^{-1}$ ];  
 $T_w$  is the wall temperature at the boundary [ $^\circ\text{C}$ ], evaluated by Equation (1);  
 $T_g$  is the gas temperature [ $^\circ\text{C}$ ] calculated by Equation (7).

The convection heat transfer coefficient is determined by the Dittus-Boelter correlation:

$$h_C = \left( \frac{k_g}{D_h} \right) 0.023 \text{Re}^{0.8} \text{Pr}^\gamma \quad (4)$$

Where:

- $k_g$  is thermal conductivity of gas [ $\text{W}\cdot\text{m}^{-1}\cdot^\circ\text{C}^{-1}$ ];  
 $D_h$  is the representative hydraulic diameter inside the flue, four times the transversal area between baffles divided by the wetted perimeter of this area [m].  
 $\text{Pr}$  is the Prandtl number of gas;  
 $\gamma$  is the exponent =0.3 for heating sections and =0.4 for cooling sections;  
 $\text{Re}$  is the Reynolds number of the flow given by:

$$\text{Re} = \frac{\dot{m}_g D_h}{A_T \mu} \quad (5)$$

- $A_T$  is the transversal area between two adjacent baffles [ $\text{m}^2$ ];  
 $\dot{m}_g$  is the gas massflow [kg/s] ;  
 $\mu$  is the dynamic viscosity of the fluid [ $\text{kg}\cdot\text{m}^{-1}\cdot\text{s}^{-1}$ ].

The radiation heat transfer coefficient is given by:

$$h_R = \sigma \left( \frac{\varepsilon_g T_g^4 - \alpha_g T_w^4}{T_g - T_w} \right) \quad (6)$$

Where:

- $\sigma$  is the Stefan-Boltzmann constant =  $5.67 \times 10^{-8}$  [ $\text{W}\cdot\text{m}^{-2}\cdot\text{K}^{-4}$ ];  
 $\varepsilon_g$  is the emissivity of mixed gas, only  $\text{H}_2\text{O}$  and  $\text{CO}_2$  are considered as they are not transparent to radiation [-];  
 $\alpha_g$  is the absorptivity of mixed gas [-], only  $\text{H}_2\text{O}$  and  $\text{CO}_2$  are considered as they are not transparent to radiation.

Detailed determination of  $\varepsilon_g$  and  $\alpha_g$  for mixed gases can be found in [6].

Temperatures of gas and solids must be calculated iteratively as they are interdependent. For the gas the thermal balance is evaluated by a one-dimensional equation, in which the velocity is high enough to neglect heat conduction inside the gas:

$$\begin{aligned} \dot{m}_g c_P \frac{\partial T_g}{\partial x} = & -\delta \frac{\partial \dot{m}_g}{\partial x} c_P (T_g - T_{\text{inf}}) - 2D_{\text{flue}} (h_C + h_R)(T_g - T_w) \\ & + \dot{m}_{f_x} H_f + \dot{m}_{\text{tar}_x} H_{\text{tar}} + \dot{m}_{\text{CH}_4_x} H_{\text{CH}_4} + \dot{m}_{\text{H}_2_x} H_{\text{H}_2} - Wh_{\text{teq}} (T_g - T_{\text{inf}}) \end{aligned} \quad (7)$$

Where:

- $\dot{m}_g$  is the flue's local gas massflow (including accumulated infiltration) [kg/s];  
 $c_P$  is the specific heat of gas [ $\text{J}\cdot\text{kg}^{-1}\cdot^\circ\text{C}^{-1}$ ];

- $\delta$  is a binary variable, =1 in underpressure zones (typically, heating sections) and = 0 in positive pressure zones (cooling sections) [-];
- $T_{inf}$  is ambient temperature [°C];
- $D_{flue}$  is the equivalent perimeter of the flue [m];
- $\dot{m}_{fx}$  is fuel massflow injection per unit of furnace length [ $\text{kg}\cdot\text{m}^{-1}\cdot\text{s}^{-1}$ ];
- $\dot{m}_{tarx}$  is the volatile tar release rate per unit of furnace length [ $\text{kg}\cdot\text{m}^{-1}\cdot\text{s}^{-1}$ ];
- $\dot{m}_{CH4x}$  is the volatile  $\text{CH}_4$  release rate per unit of furnace length [ $\text{kg}\cdot\text{m}^{-1}\cdot\text{s}^{-1}$ ];
- $\dot{m}_{H2x}$  is the volatile  $\text{H}_2$  release rate per unit of furnace length [ $\text{kg}\cdot\text{m}^{-1}\cdot\text{s}^{-1}$ ];
- $H_f$  is the heat of reaction of fuel [J/kg];
- $H_{tar}$  is the heat of reaction of volatile tar [J/kg];
- $H_{CH4}$  is the heat of reaction of volatile  $\text{CH}_4$  [J/kg];
- $H_{H2}$  is the heat of reaction of volatile  $\text{H}_2$  [J/kg];
- $W$  is the flue width [m];
- $h_{teq}$  is the equivalent heat transfer coefficient which takes into account the conductive resistance of the top block and the convective and irradiative heat transfer from the top block to the atmosphere [ $\text{W}\cdot\text{m}^{-2}\cdot\text{°C}^{-1}$ ].

The mass flow of the species is also evaluated by the balance ( $\text{O}_2$ ,  $\text{CO}_2$  and  $\text{H}_2\text{O}$ ) equations:

$$\frac{\partial(\dot{m}_{O_2})}{\partial x} = -R_{O_2-f}\dot{m}_{fx} + 0.232\delta\frac{\partial\dot{m}_g}{\partial x} - R_{O_2-tar}\dot{m}_{tarx} - R_{O_2-CH_4}\dot{m}_{CH4x} - R_{O_2-H_2}\dot{m}_{H2x} \quad (8)$$

$$\frac{\partial(\dot{m}_{CO_2})}{\partial x} = R_{CO_2-f}\dot{m}_{fx} + 0.00053\delta\frac{\partial\dot{m}_g}{\partial x} + R_{CO_2-tar}\dot{m}_{tarx} + R_{CO_2-CH_4}\dot{m}_{CH4x} + R_{CO_2-H_2}\dot{m}_{H2x} \quad (9)$$

$$\frac{\partial(\dot{m}_{H_2O})}{\partial x} = R_{H_2O-f}\dot{m}_{fx} + 0.0062\delta\frac{\partial\dot{m}_g}{\partial x} + R_{H_2O-tar}\dot{m}_{tarx} + R_{H_2O-CH_4}\dot{m}_{CH4x} + R_{CO_2-H_2}\dot{m}_{H2x} \quad (10)$$

Where:

- $\dot{m}_{O_2}$  is the oxygen massflow passing through the flue [kg/s];
- $\dot{m}_{CO_2}$  is the carbon dioxide massflow passing through the flue [kg/s];
- $\dot{m}_{H_2O}$  is the water vapor massflow passing through the flue [kg/s];
- $R_{a-b}$  is the ratio of proportionality, in mass, of a component "a" with respect to a component "b" in the chemical reaction.

We assume that combustion of fuel and volatiles is fast and occurs immediately after these substances enter the flue space. The concentrations are evaluated by dividing the species volume flow by total volume flow of gases at each calculation point.

### Gas Massflow

For correct calculation of temperature and oxygen balance, the gas massflow and infiltration profiles must be known. These quantities are a function of the draft imposed on the system, the flue cavity design and furnace sealing at the headwall cover, peep-hole covers, open brick joints and packing coke.

The gas flow along the flues is considered as a flow in a pipe, where the pressure distribution is governed by the equation of hydraulic loss:

$$\frac{\partial P}{\partial x} = \frac{T_g K}{L_{flue}} (\dot{m}_g)^2 \quad (11)$$

Where:

$P$  is static pressure inside the flue [Pa];

$L_{flue}$  is the length of one section in the x direction [m];

$K$  is the hydraulic resistance of one flue [ $\text{kg}^{-1} \cdot \text{m}^{-1} \cdot \text{K}^{-1}$ ].

$\dot{m}_g$  is gas massflow [kg/s].

The dynamic pressure term  $\frac{\partial}{\partial x}(\rho V^2)$  is neglected.

### Hydraulic Resistance

This must be determined by experiment or by 3D fluid flow simulation. According to hydraulic theory, in general, hydraulic components and canalizations obey the following relationship:

$$\Delta P = K_T \dot{m}_g^2 \quad (12)$$

Where:

$\Delta P$  is the pressure drop when the fluid passes through the component [Pa];

$K_T$  is a constant of proportionality.  $K_T$  is valid for a given fluid temperature [ $\text{kg}^{-1} \cdot \text{m}^{-1}$ ].

In the case of ideal gases a general  $K$  is proposed which is valid for any temperature:

$$K = \frac{K_T}{T_g} \quad (13)$$

Where:

$T_g$  is the fluid temperature [K].

$K$  is a characteristic of the flue geometry design only [ $\text{kg}^{-1} \cdot \text{m}^{-1} \cdot \text{K}^{-1}$ ].

A 3D fluid flow model of one section of the flue wall, considering only half due to the symmetry of the cavity width, is used to determine hydraulic resistance. As a boundary condition, an arbitrary massflow is chosen resulting in a pressure drop. By applying Equation 12 and 13, we obtain  $K$  which is valid for any massflow or pressure drop at any temperature.

As an example, Figure 3(a) presents the fluid flow streamlines inside a flue cavity for a massflow of 0.2 kg/s at 600°C. Figure 3(b) presents the resulting pressure field inside the flue cavity. The resulting pressure drop is 25.8 Pa and the calculated hydraulic resistance ( $K$ ) was  $0.739 \text{ kg}^{-1} \cdot \text{m}^{-1} \cdot \text{K}^{-1}$  for the half flue cavity width.

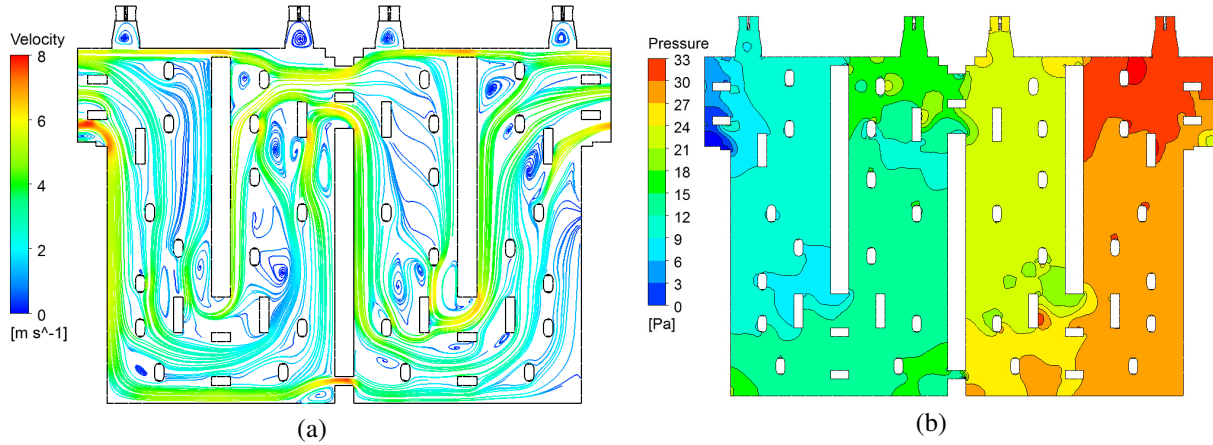


Figure 3 – Fluewall Fluid Flow Velocities Streamlines (a) and Pressure Drop (b).

### Air Infiltration

The amount of air infiltration from the atmosphere depends on the local flue underpressure and the hydraulic resistance between flue and atmosphere due to furnace sealing, open brick joints and packing coke permeability. An equation similar to Equation (12) can be written:

$$P = -K_{inf} I_x^2 \quad (14)$$

Where:

$P$  is the underpressure inside the flues [Pa];

$K_{inf}$  is the hydraulic resistance to infiltration over a certain porous area [ $\text{kg}^{-1} \cdot \text{m}^1$ ], which is determined by experimental data of underpressure profile;

$I_x$  is the amount of air infiltration per furnace length [ $\text{kg} \cdot \text{s}^{-1} \cdot \text{m}^{-1}$ ];

The infiltration along the furnace can be expressed also as in [2]:

$$I_x = -\frac{\partial \dot{m}_g}{\partial x} \quad (15)$$

The hydraulic resistance to infiltration could be determined by experimental data of underpressure profile inside the fluewall using Equation 14. Different furnaces can have more or less efficient sealing. This is expressed in the different infiltration hydraulic resistances. Our experience in ten different furnaces showed that this coefficient could vary from  $3 \times 10^6$  to  $4 \times 10^7$ .

In the example of the Figure 4 the infiltration resistance of  $K_{inf} = 4 \times 10^6$  results in a pressure profile in agreement with measurements. We ran two other models, one with extremely high infiltration resistance coefficient ( $K_{inf} = \text{infinity}$ ) resulting in a perfect sealed furnace, and the other with very low infiltration resistance ( $K_{inf} = 3.6 \times 10^5$ ). As we can see in the figure both result in a profile that did not match the measurements. The correct infiltration resistance is important to obtain the correct gas temperature at pre-heating, the resulting fuel consumption as well as the anode temperature.

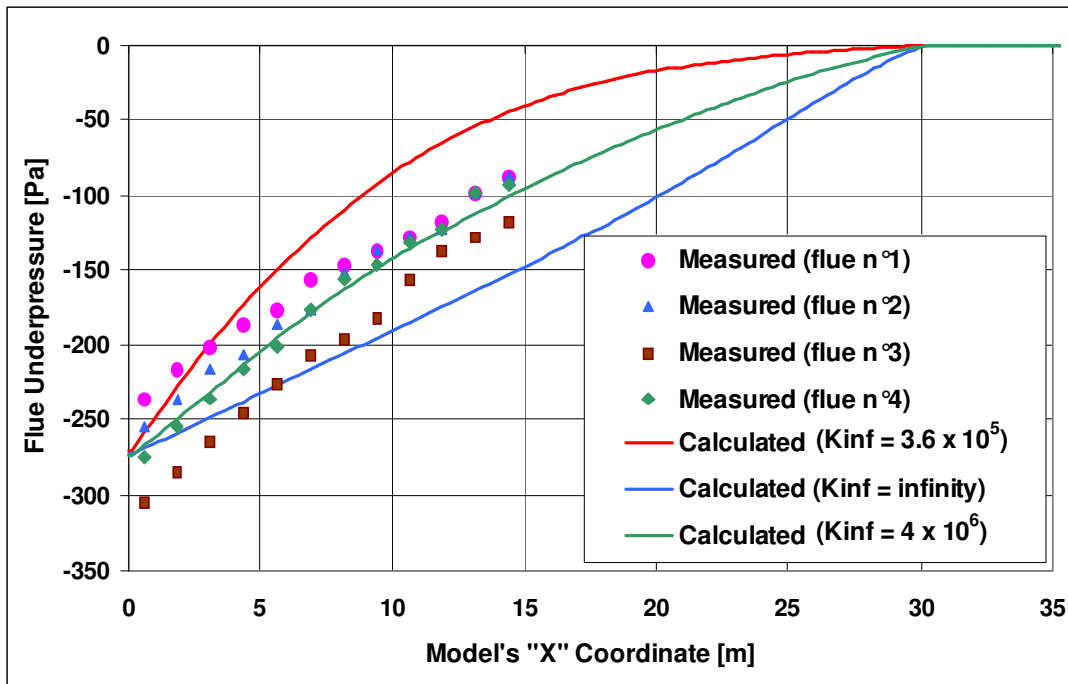


Figure 4 - Flue Underpressure Measurements (Points) and Calculated Profiles (Lines) with Different Infiltration Resistances.

Combining Equation (12) to Equation (15) we obtain infiltration as a function of pressure, massflow and infiltration profiles. The Figure 5 presents the modeling underpressure and gas massflow at each point inside the furnace applying this methodology for a given furnace.

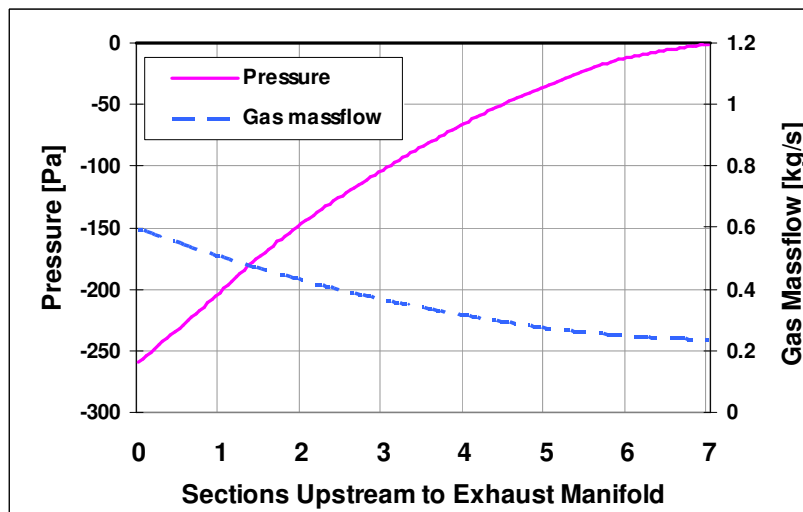


Figure 5 - Underpressure and Gas Massflow for a Given Furnace with Air Infiltration.

### Volatiles Release Rate

The amount of power obtained from volatile burn is a function of the anode temperature, and the mass of volatiles stored in the green anodes. Mathematically the volatiles release rates are expressed as:

$$\dot{m}_{tarx} = \frac{\partial m_{tarx}}{\partial T_a} \frac{\partial T_a}{\partial t} \quad (16)$$

$$\dot{m}_{CH_4x} = \frac{\partial m_{CH_4x}}{\partial T_a} \frac{\partial T_a}{\partial t} \quad (17)$$

$$\dot{m}_{H_2x} = \frac{\partial m_{H_2x}}{\partial T_a} \frac{\partial T_a}{\partial t} \quad (18)$$

Where:

$T_a$  is the anode temperature at a given coordinate.

The anode temperature rate is  $\frac{\partial T_a}{\partial t}$  obtained during the simulation.

The volatiles conversion rates  $\frac{\partial m_{tarx}}{\partial T_a}$ ,  $\frac{\partial m_{CH_4x}}{\partial T_a}$ ,  $\frac{\partial m_{H_2x}}{\partial T_a}$  are given by published laboratory measurement data [7]. These data are fitted with exponential curves:

$$\frac{\partial m_{tarx}}{\partial T_a} = 26.21 F_{tar} e^{\frac{-10452}{RT_a}} (1 - X_{tar})^{1.5} \quad (19)$$

$$\frac{\partial m_{CH_4x}}{\partial T_a} = 3.59 * 10^8 F_{CH_4} e^{\frac{-41871}{RT_a}} (1 - X_{CH_4})^{2.0} \quad (20)$$

$$\frac{\partial m_{H_2x}}{\partial T_a} = 22000 F_{H_2} e^{\frac{-30043}{RT_a}} (1 - X_{H_2})^{1.5} \quad (21)$$

Where:

$X_{tar}$ ,  $X_{CH_4}$ ,  $X_{H_2}$ , are the fractions of conversion of tar, CH<sub>4</sub> and H<sub>2</sub>, respectively, going from 0 to 1 [-] ;

$F_{tar}$ ,  $F_{CH_4}$ ,  $F_{H_2}$ , are the total amount of volatile mass to be released by the anodes per unit of length [kg/m];

$R$  is the universal gas constant [J.K<sup>-1</sup>.mol<sup>-1</sup>];

The model applies the heat sources in the flue volume according to the current anode average temperature following the equations (16) to (21), resulting in the curves of the Figure 6.

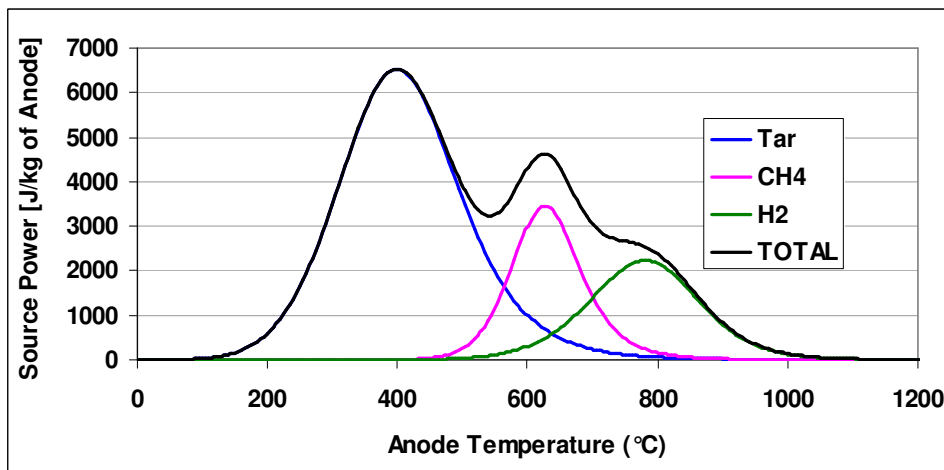


Figure 6 - Power Released by each Volatile as a Function of the Anode Temperature

## Validation

The furnace operation data and measurements from several different furnace designs known by the authors have been compared with the behavior predicted by the numerical models in different aspects. The Figure 7 shows measured underpressure inside the flue cavities versus calculation results. The calculated underpressure profile was obtained by the model using appropriate resistance parameters between flue chamber and atmosphere.

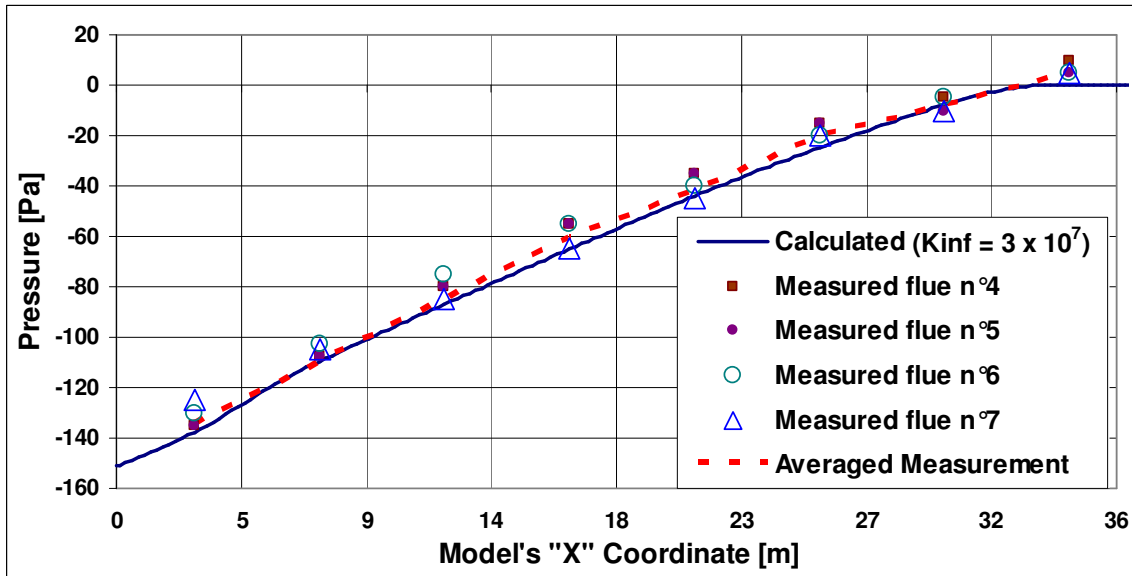


Figure 7 - Comparison of Measured and Calculated Underpressure inside the Flues

The Figure 8 shows the comparison between the averaged measured and modeled anode temperatures. The temperatures were measured using thermocouples installed inside the packing coke between the flue wall and anodes.

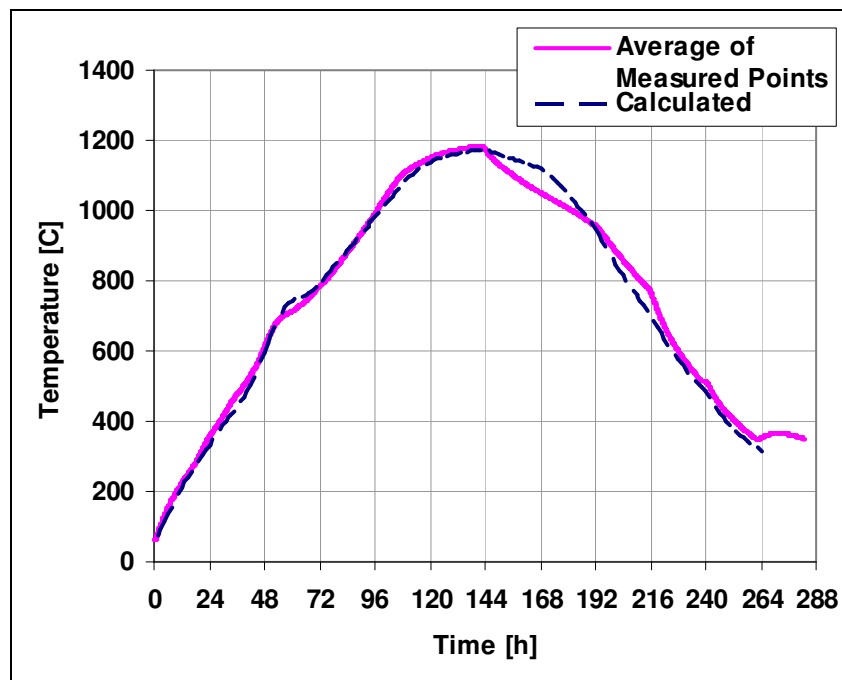


Figure 8 - Measured and Calculated Temperatures inside the Packing Coke [10]

The Figure 9 shows the gas temperature calculated and measured by the control system inside the flue chamber in the peepholes. Sections 2 and 3 are pre-heating and 4 to 5 are firing. We can notice the very good correlation in the 3<sup>rd</sup> section where the volatiles peak occurs.

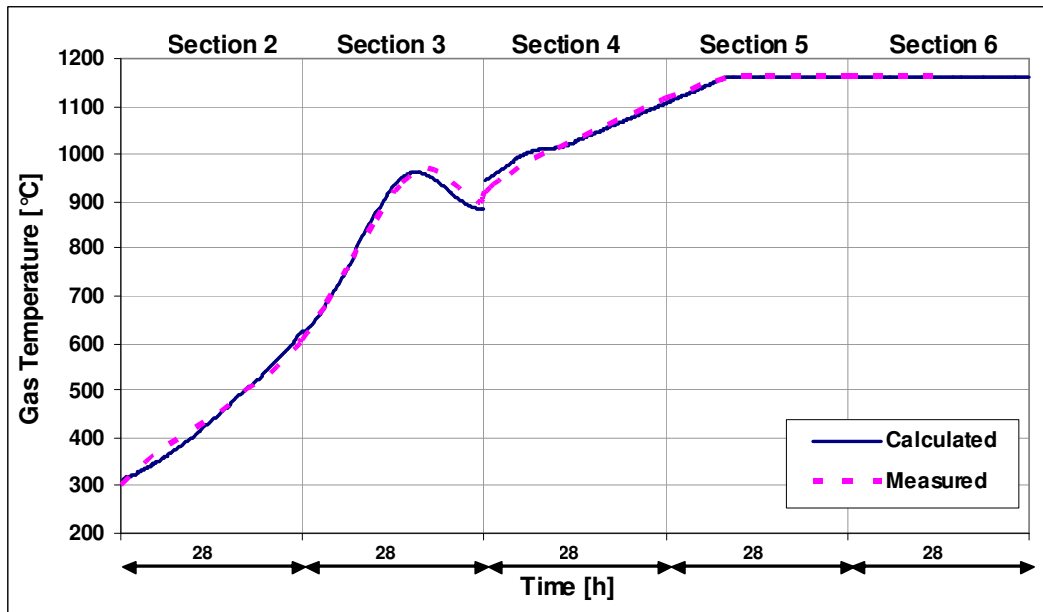


Figure 9 - Comparison of Measured and Calculated Flue Gas Temperatures during the Baking Process

Another way to check the model is by comparing the model predicted fuel consumption in [GJ/ton] of baked anodes with the plant informed fuel consumption per ton of anode averaged per month during one year. Figure 10 shows the comparison between the consumption reported by plant and predicted by modeling. We must observe that in real furnaces a small part of the energy is lost in the crossovers and through furnace sidewalls. These losses are not included in the model. This could explain the slightly higher consumption reported in comparison with the predicted in most cases. However the prediction is inside the variability presented by the data and can be considered a valid prediction.

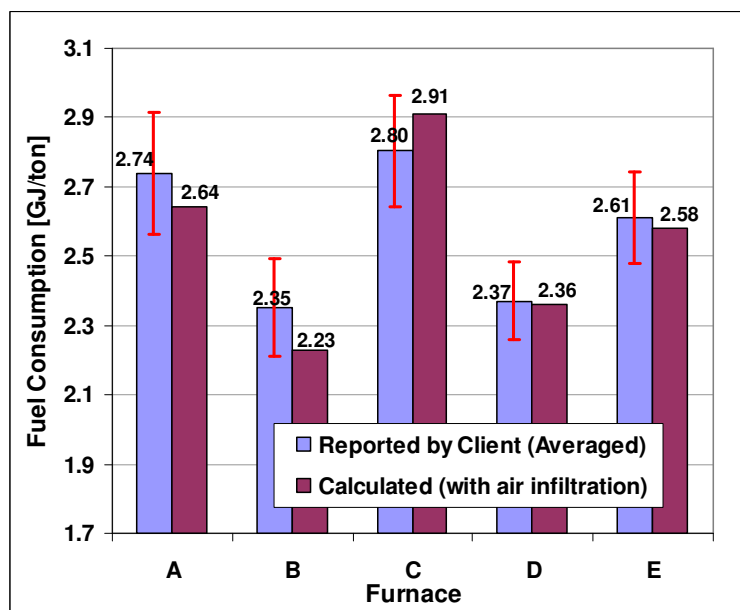


Figure 10 - Fuel Consumption in GJ/Ton of Produced Anodes for Five Different Furnaces, with Averages and Standard Deviation Limits, Compared with Predicted Value by the Software

## Case Study

A generic furnace is presented to illustrate the use of the software. The pit size and flue wall design are internal constants that are part of the software setup and could not be modified by the user. Three cases are presented in this paper. In the Case 1 and 2 constant massflow is used to have minimum Oxygen of around 8% all the time. Case 3 is a test with variable draft following an exhaust temperature control curve.

The case study furnace characteristics are:

- Anode pack size: 4550mm of length, 4500mm of height and 600mm of width.
- Pit dimensions: 5350mm of length, 5100mm of height and 750mm of width.
- Length of one section including headwalls: 5750mm
- Number of sections: 3 in preheating, 3 in firing and 5 in cooling.
- Zero relative pressure location: 1 cooling section at downstream
- Anode top coke thickness: 600mm
- Infiltration hydraulic resistance:  $4 \times 10^6$  [m/kg].
- Flue wall hydraulic resistance:  $0.75$  [ $\text{m}^{-1} \cdot \text{K}^{-1} \cdot \text{kg}^{-1}$ ]
- Cooling fan 1: massflow 1.2 kg/s; located at 2 sections upstream of back burner bridge.
- Cooling fan 2: massflow 2.0 kg/s; located at 4 sections upstream of back burner bridge.
- Ambient temperature: 30°C;
- Fire control curve: initial temperature of 940°C and final temperature of 1180°C;
- Burned volatiles as fraction of the anode mass: 3.4wt% of tar, 0.36wt% of H<sub>2</sub> and 0.9wt% of CH<sub>4</sub>.
- Cycle time: 24h for Cases 1 and 3; 28h for Case2;
- Soaking time: 36h for Cases 1 and 3; 42h for Case2;
- Exhaust temperature control curve for Case 3: initial temperature of 420°C and final temperature of 810°C;
- Allowable underpressure at draft bridge for Case 3: minimum of 50Pa and maximum of 300 Pa;
- Material properties according to the Table 1.

*Table 1 - Material Properties Used in the Study Cases*

Material	Thermal Conductivity [W.m <sup>-1</sup> .K <sup>-1</sup> ]	Specific Heat [J.kg <sup>-1</sup> .K <sup>-1</sup> ]	Density [kg/m <sup>3</sup> ]
Refractory bricks	1.46	965	2490
Concrete	1.4	2300	880
Soil	2.2	2050	1840
Packing coke			
20°C	0.87	652	1240
100°C	0.87	941	1240
300°C	0.95	1374	1240
500°C	1.08	1650	1240
700°C	1.24	1816	1240
1000°C	1.50	2000	1240
Anode			
20°C	2.55	871	1545
200°C	2.45	1105	1545
500°C	3.75	1291	1545
700°C	4.55	1311	1545
850°C	5.30	1414	1545
1000°C	6.05	1519	1545
1200°C	7.00	1700	1545

Figure 11 and 12 show the software user interface.

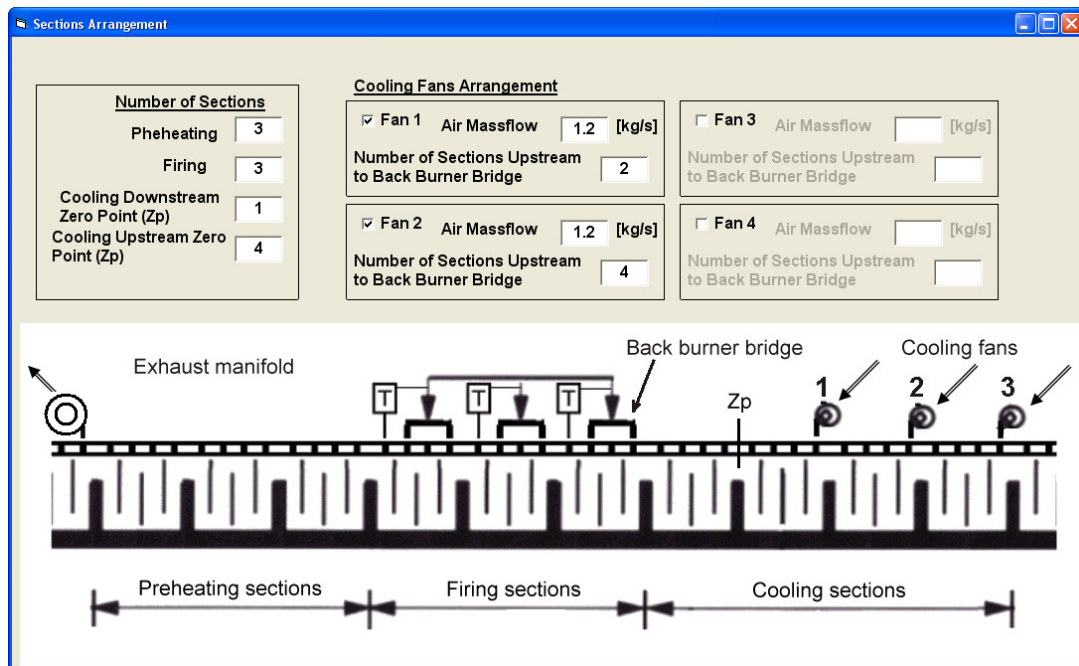


Figure 11 – Software Input Data Screen

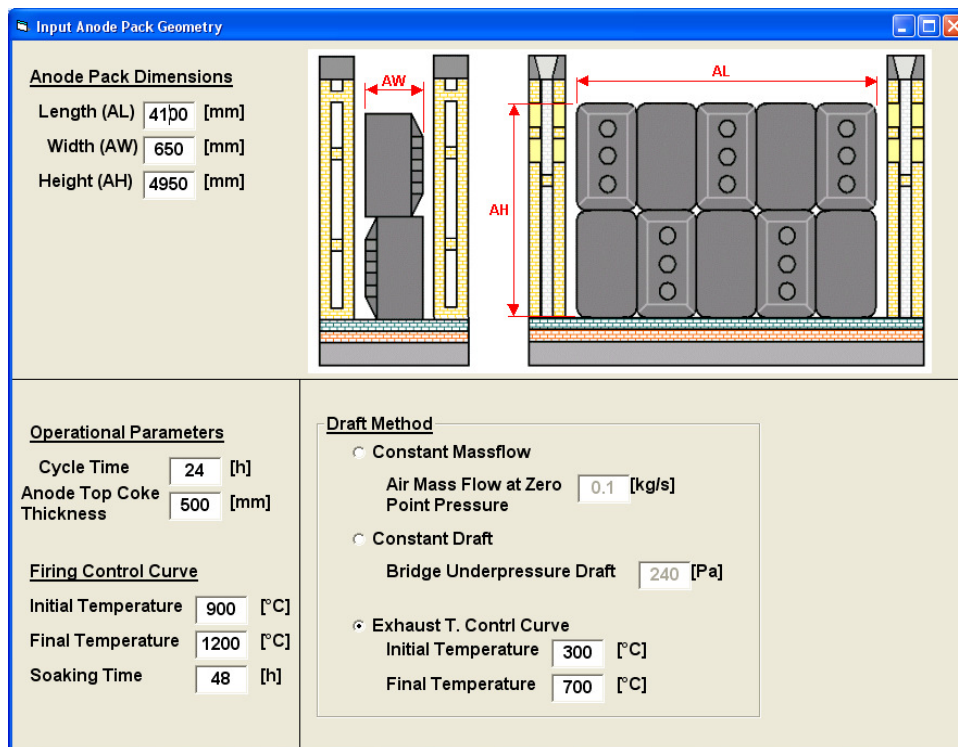


Figure 12 – Software Input Data Screen

## Results

The Table 2 summarizes some model results for the three cases. The furnace energy efficiency was calculated dividing the energy stored in the anodes by the sum of the energy from volatiles and fuel. We can notice the large amount of energy that is wasted through the exhaust gases and also that used to heat-up the solids such as flue wall, coke and others. These losses are responsible for the relatively low energy efficiency of this type of furnace.

Table 2 – Compilation of the Results from the Model

	Case 1	Case 2	Case 3
Minimum Oxygen [%]	7.92	8.04	4.53
Fuel consumption [GJ/ton]	2.14	2.38	2.10
Energy from volatiles [GJ/ton]	2.19	2.19	2.19
Energy recovered from cooling [GJ/ton]	0.97	1.04	0.96
Energy stored in the anodes [GJ/ton]	1.58	1.64	1.58
Energy waste at exhaust [GJ/ton]	1.00	1.07	0.94
Energy losses to foundation [GJ/ton]	0.08	0.08	0.08
Energy losses to ambient [GJ/ton]	0.15	0.17	0.15
Energy losses to heat-up solids [GJ/ton]	2.49	2.65	2.50
Furnace energy efficiency [%]	36.5	35.8	36.8
Underpressure at section 1 peephole A [Pa]	235	189	224
Draft bridge underpressure at section 3 peephole B [Pa]	127	102	121
Air massflow at zero relative pressure location [kg/s]	0.135	0.121	0.131
Gas massflow leaving section 1 [kg/s]	0.311	0.278	0.302
Anode pack average final temperature [°C]	1047	1072	1047
Maximum gas temperature at section 1 peephole A [°C]	512	522	471
Maximum gas temperature at section 1 peephole D [°C]	804	782	810

Increasing cycle time from 24h to 28h (Case 1 versus 2) increases anode final temperature by 25°C and reduces the draft required by almost 20%, but increases fuel consumption by 0.24 GJ/ton. Using the exhaust temperature control curve (Case 3) reduces the fuel consumption by 0.04 GJ/ton when comparing with Case 1 while keeping the same anode final temperature, but increases the risk of soot formation since the minimum Oxygen available reduces to 4.5%.

Figure13 shows gas temperature evolution at peephole B during the baking process. Also the anode pack average temperature is plotted. We can see the volatiles peak difference between Case 1 and 2 and also the high final anode temperature for Case 2 due to its longer cycle time.

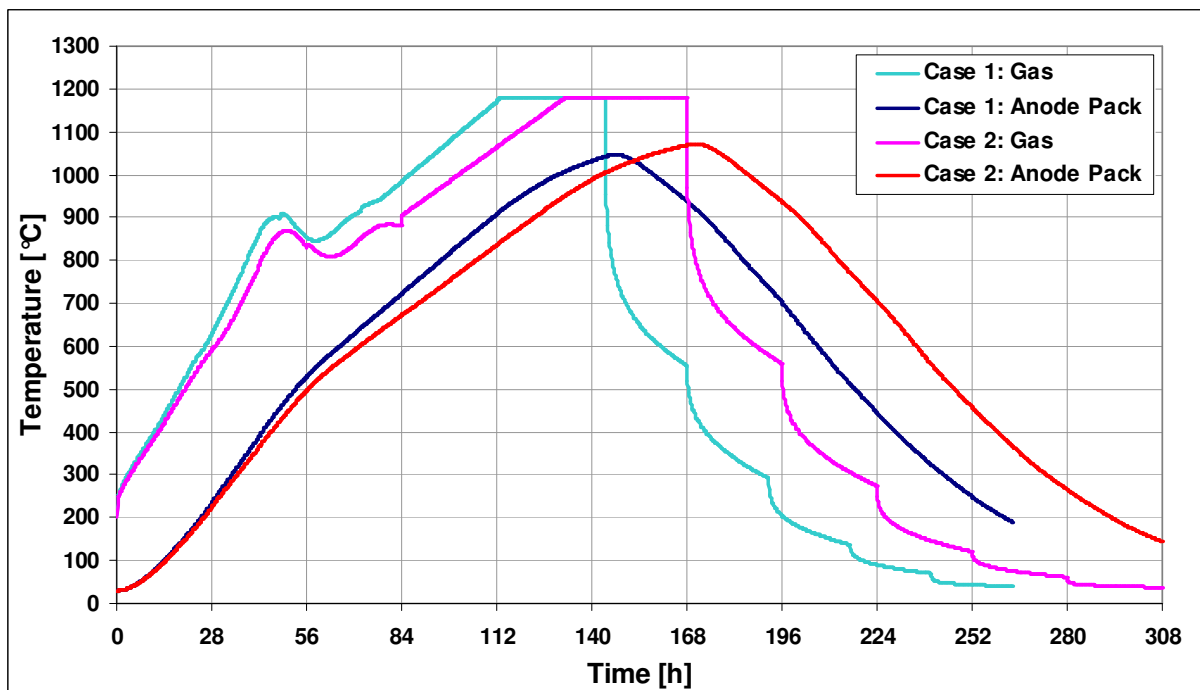


Figure 13 – Case 1 and 2 Calculated Gas Temperature at Peephole B and Anode Pack Average Temperature

Figure 14 shows the comparison between Case 1 and 3 where despite the different strategy – constant massflow versus exhaust gas control – the anode and gas temperature results in almost the same behavior during the process.

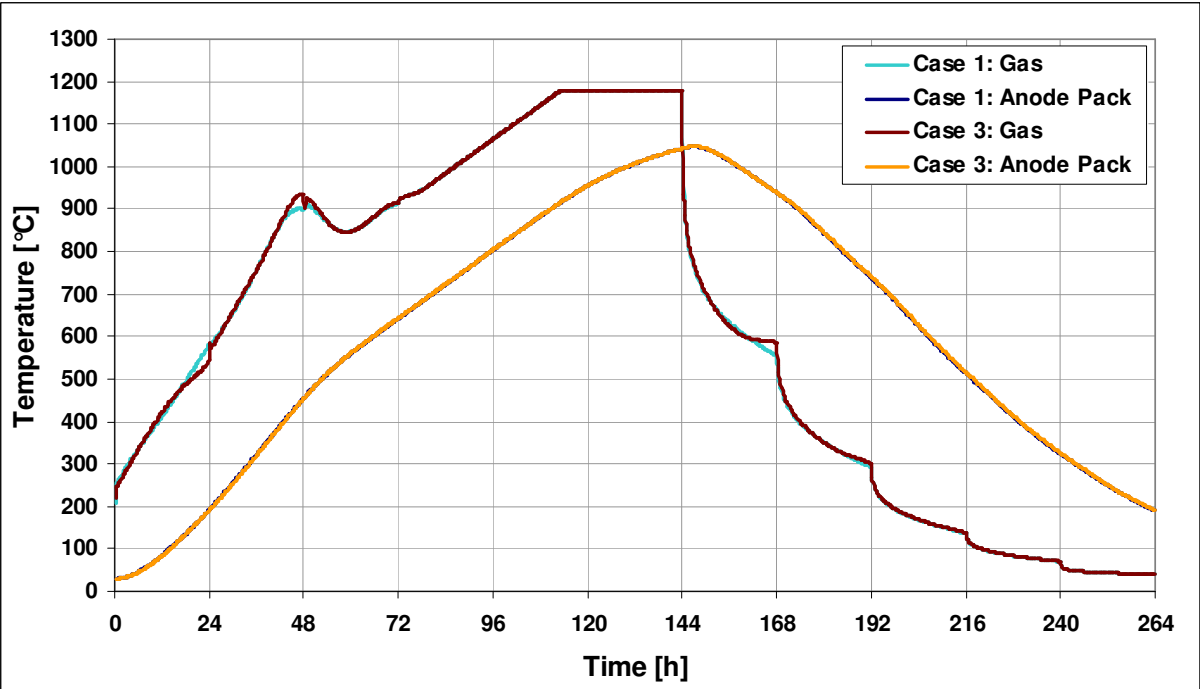


Figure 14 – Case 1 and 3 Calculated Gas Temperature at Peephole B and Anode Pack Average Temperature

The Figure 15 shows the released volatiles energy along the sections at the instant when the minimum Oxygen level is reached, for Case 1 and 2. We can see volatiles being released and burned even at the firing sections. In the model the volatiles are not released at the headwalls, and this explains the zero values at the beginning and end of each section.

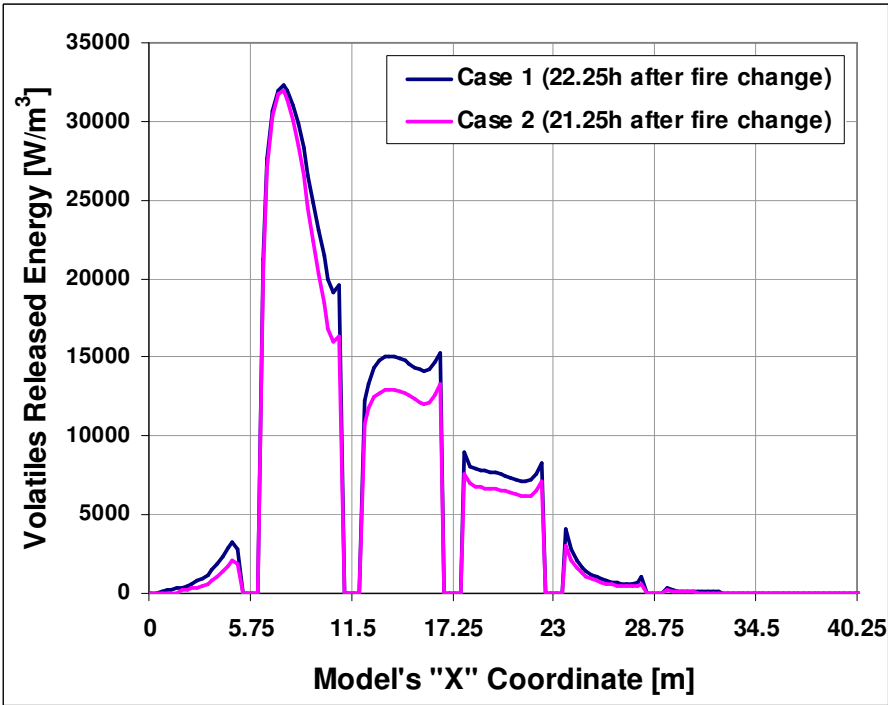


Figure 15 – Released Volatiles Energy in the Sections when the Minimum Oxygen is Reached.

The Figure 16 shows the underpressure obtained during the cycle time for the three cases in the section 3 peephole B where the draft bridge is usually located. We can see the Case 3 variable underpressure in order to achieve the target exhaust gas temperature.

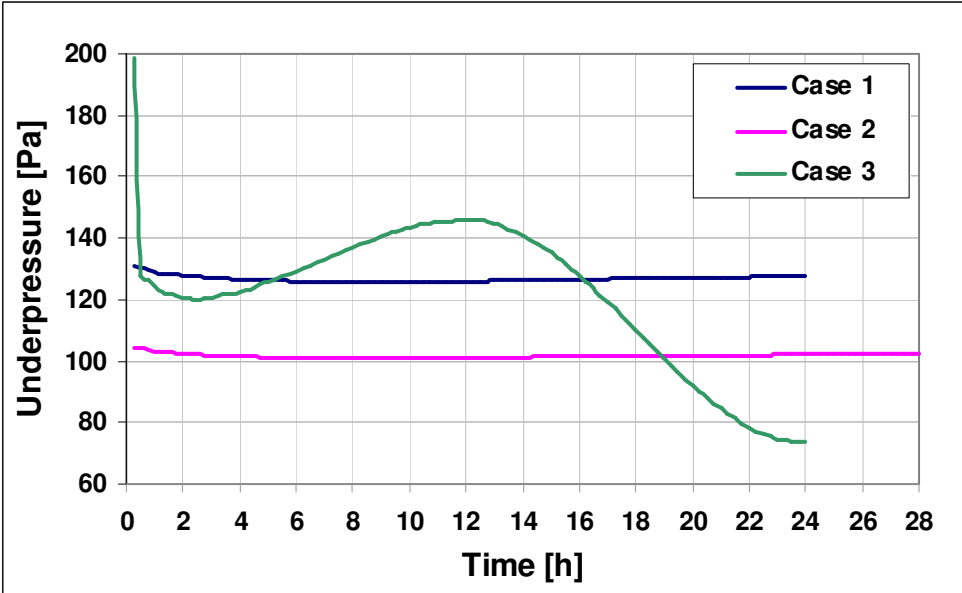


Figure 16 – Underpressure at Section 3 Peephole B for all Cases.

The Figure 17 shows the minimum Oxygen in the pre-heating sections during the cycle time for the three cases. We can see that the Case 3 variable underpressure is the one that presents the bigger variation. This occurs because at the end of the fire cycle the control system tries to follow the exhaust temperature curve by reducing the underpressure, and as a consequence the massflow, which will reduce the Oxygen supply to the pre-heating sections.

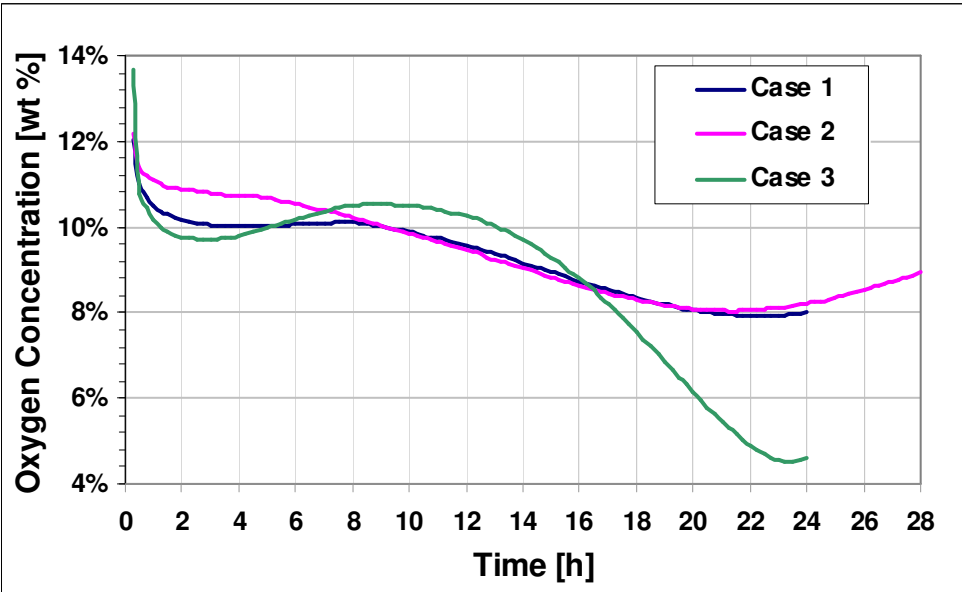


Figure 17 – Minimum Oxygen Concentration in the Pre-Heating Sections.

The Figure 18 shows a snapshot of the Oxygen concentration (wt %) along the sections at the instant when the minimum level is reached, for Case 1 and 3. This study is very important since the lack of Oxygen will increase the risk of incomplete combustion of the pitch volatile matter, forming soot and tar deposits in the exhaust manifold and ducts. This is also linked to the final fuel consumption.

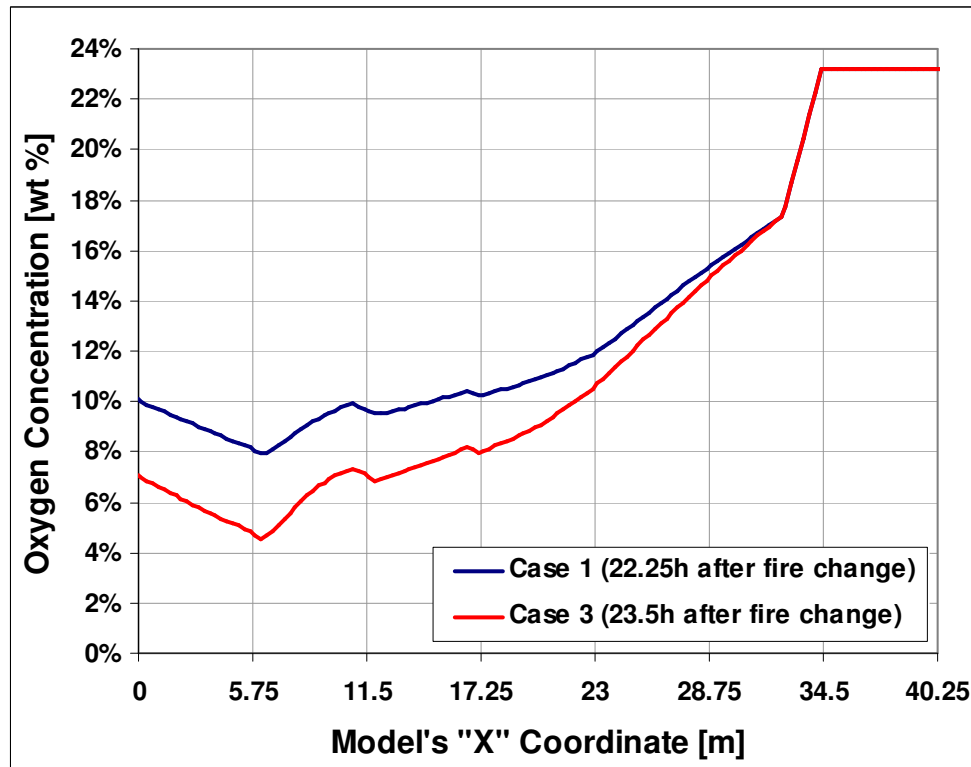


Figure 18 – Oxygen Concentration along the Sections when the Minimum is Reached.

## Conclusions

Anode baking is a very complex process, and a mathematical model is a good tool for understanding the process. This improved understanding will then lead to better furnace control strategies.

We believe this model represents the process very well. It is easy and fast enough to be used for process improvements by plant process engineers. Operational parameters such as fire cycle, temperature control curves and draught can be easily tested, and their impact on the volatiles combustion and final anode temperature assessed before implementation. This reduces the cost and risk of trials.

The model can be used as a tool to maximize the production of the anode baking furnace, improve anode quality, increase overall energy efficiency and lower the emissions. The impact of anode size changes can also be tested in advance.

The anode baking process, and the quality of the anodes produced, are critical elements of an efficient aluminium smelter. This software can be used to optimize the anode baking process from both cost and quality perspectives.

## References

- [1] Ulrich Mannweiler, *Anodes for the Aluminium Industry* (Sierre, Switzerland: R&D Carbon Ltd., 1<sup>st</sup> Edition, 1995), 197-202.
- [2] R. T. Bui, E. Darnedde, A. Charette and T. Bourgeois, “Mathematical simulation of horizontal flue ring furnace”, *Light Metals* (1984), 1033-1040.
- [3] R. Ouellet, Q. Jiao, E. Chin, C. Celik, D. Lancaster and D. Wilburn, “Anode baking furnace modelling for process optimization”, *Light Metals* (1995), 653-662.
- [4] V. Potocnik, G. Asadi and G. Poulin, “Analysis of horizontal anode baking furnace flue designs”, *Recent Metallurgical Advances in Light Metals Industries - 34<sup>th</sup> Annual Conference of Metallurgists of CIM* (1995), 157-166.
- [5] Y.F. Kocaefe, E. Darnedde, D. Kocaefe, R. Ouellet, Q. Jiao and W. F. Crowell, “A 3D mathematical model for the horizontal anode baking furnace”, *Light Metals* (1996), 529-534.
- [6] F. P. Incropera, D. P. De Witt, *Fundamentals of Heat and Mass Transfer*, 4<sup>th</sup> Edition, Chapter 9, 1996.
- [7] A. D. Tomsett, "The Role of Pitch Volatiles in Anode Baking", *8th Australasian Aluminium Smelting Conference and Workshops* (2004), 436-446.
- [8] D.S. Severo, V. Gusberti and E.C.V. Pinto, “Advanced 3D Modeling for Anode Baking Furnaces”, *Light Metals* (2005), 697-702.
- [9] Felix Keller, Peter Sulger, Markus Meier, Dagoberto S. Severo and Vanderlei Gusberti, “Specific Energy Consumption in Anode Bake Furnaces”, *Light Metals* (2010), 1005-1010.
- [10] Dagoberto S. Severo, Vanderlei Gusberti, Peter Sulger, Felix Keller and Dr. Markus Meier, “Recent Developments in Anode Bake Furnace Design”, *Light Metals* (2011), 853-858.